aforementioned heating rate and dust radiative forcing can be gained from comparison of the rate of absorption of solar radiation by the dust layer. For example, our measurements from Cape Verde (16.7° N, 23° W) for 1994–95 suggest an average optical thickness of 0.35 for the dust layer. The heating rate in the 650–850 hPa layer for $\tau = 0.35$ can be estimated from ref. 19 (see their Figs 12, 13) by interpolating values given for $\tau = 0.2$ and $\tau = 0.5$. This procedure gives heating rates of 0.1–0.2 K d^{-1} for the cloud-free ocean case, and up to 0.3–0.5 K d^{-1} in the cloud case, which fits well with our estimations for an average dust event of 0.21 K d^{-1} or 0.19 K d^{-1} (derived from Figs 3 and 4, respectively).

Another comparison can be made with most recent modelling results from Tegen *et al.*[3], who indicate that the average mean global optical thickness coming from disturbed soil is 0.017. To retrieve our mean value (0.35), we have to assume that dust with $\tau = 0.35$ is covering 5% of the total Earth's surface. As dust is located between 10° and 30° N, approximately one-third of the 10–30° latitude belt would be covered by a dust cloud of $\tau = 0.35$. They further indicate that the longitudinal mean heating between 10° and 30° N is 0.04 K d^{-1}: this would result in a heating rate that is three times larger where dust is located, or 0.12 K d^{-1}.

There is also a dynamical heating effect on the IAU due to the Saharan air layer (SAL). This, however, has a different spatial and temporal signature from dust and concentrates in a lower-altitude layer[20]. The sporadic heating due to the dust at a particular time and location is determined by the transient local properties of a travelling dust plume—the local dust profile and dust content—whereas that of the SAL is on a larger (synoptic) scale. Therefore, dust plume heating is superposed locally and perhaps semirandomly on that of the SAL. The model is sensitive to the general presence and intensity of the SAL but does not contain dust. The product of the data assimilation system—the IAU—does include the effects of dust and thus can show the much more rapidly variations in local conditions due to the passing of a dust plume. Also, the vertical profiles of both the IAU and the theoretical diabatic heating due to Saharan dust[19] show a sharp increase in the 750–580 hPa layer which is located with the average upper part of the dust layer; the climatological SAL profiles, however, indicate a peak in the heating rate below 900 hPa.

We have also compared the global seasonal IAU(T) for 1987 with equivalent atmospheric optical thicknesses (EAOT) maps from Husar *et al.*[8]: this indicates that the pattern similarities between IAU(T) and EAOT exist not only over the Atlantic Ocean but also over other dusty regions, including the Indian Ocean, the Bay of Bengal and the south China Sea during spring and summer (not shown).

This work indirectly shows the response of the temperature field to the radiative forcing of the dust layer. The resulting heating rate of 6 K yr^{-1} within the dust layer at 1.5–3.5 km is in agreement with calculated heating rates[17,20–22] and therefore may be used for improving atmospheric predictions once dust loading is monitored daily by satellite, as is planned for the MODIS (Moderate Resolution Imaging Spectroradiometer) instrument on the Earth-observing system[23,24]. □

Received 16 April 1997; accepted 3 July 1998.

1. Charlson, R. *et al.* Climate forcing by anthropogenic aerosols. *Science* **255**, 423–430 (1992).
2. Penner, J. E. *et al.* Quantifying and minimizing uncertainty of climate forcing by anthropogenic aerosols. *Bull. Am. Meteorol. Soc.* **75**, 375–400 (1994).
3. Tegen, I., Lacis, A. A. & Fung, I. The influence of mineral aerosols from disturbed soils on the global radiation budget. *Nature* **380**, 419–422 (1996).
4. Arking, A. The radiative effects of clouds and their impact on climate. *Bull. Am. Meteorol. Soc.* **72**, 795–813 (1991).
5. Lindzen, R. S. Some coolness concerning global warming. *Bull. Am. Meteorol. Soc.* **71**, 288–299 (1990).
6. Moulin, C., Lambert, C. E., Dulac, F. & Dayan, U. Control of atmospheric export of dust from North Africa by the North Atlantic Oscillation. *Nature* **387**, 691–694 (1997).
7. Prospero, J. M. *et al.* Temporal variability of summertime ozone and aerosols in the free troposphere over the eastern North Atlantic. *Geophys. Res. Lett.* **22**, 2925–2928 (1995).
8. Husar, R. B., Prospero, J. M. & Stowe, L. L. Characterization of tropospheric aerosols over the oceans with the NOAA advanced very high resolution radiometer optical thickness operational product. *J. Geophys. Res.* **102**, 16889–16910 (1997).
9. Daley, R. *Atmospheric Data Analysis* (Cambridge Univ. Press, New York, 1991).
10. Bloom, S. S., Takacs, L. L., da Silva, A. M. & Ledvina, D. Data assimilation using incremental analysis updates. *Mon. Weath. Rev.* **124**, 1256–1271 (1996).
11. Schubert, S. *et al.* An assimilated data set for Earth Science applications. *Bull. Am. Meteorol. Soc.* **74**, 2331–2342 (1993).
12. Jankoviak, I. & Tanre, D. Satellite climatology of Saharan dust outbreaks: Method and preliminary results. *J. Clim.* **15**, 646–656 (1992).
13. Prospero, J. M. & Nees, R. T. Impact of the North African drought and El Niño on the mineral dust in the Barbados trade winds. *Nature* **320**, 735–738 (1986).
14. Westphal, D. L., Toon, O. B. & Carlson, T. N. A two-dimensional numerical investigation of the dynamics and micro-physics of Saharan dust storms. *J. Geophys. Res.* **92**, 3027–3049 (1987).
15. Rossow, R. B. & Schiffer, R. A. ISCCP cloud data products. *Bull. Am. Meteorol. Soc.* **72**, 2–20 (1991).
16. Asnani, G. C. *Tropical Meteorology* (Indian Inst. of Tropical Meteorology, Pune, 1993).
17. Pick, C. *Transport of Desert Aerosols and their Influence on Local Temperature and Motion.* Thesis, Tel Aviv Univ. (1991).
18. Eubank, R. L. *Spine Smoothing and Non-parametric Regression* (Dekker, New York, 1988).
19. Carlson, T. N. & Benjamin, S. G. Radiative heating rates for Saharan dust. *J. Atmos. Sci.* **37**, 193–213 (1980).
20. Karyampudi, V. M. *A Numerical Study of the Evolution, Structure and Energetics of the Saharan Air Layer.* Thesis (Pennsylvania State Univ., 1986).
21. Joseph, J. H. in *Aerosols and their Climatic Effects* (eds Gerber, H. E. & Deepak, A.) 215–226 (Deepak, Hampton, VA, 1984).
22. Alpert, P. & Ganor, E. A jet-stream associated heavy dust storm in the western Mediterranean *J. Geophys. Res.* **98**, 7339–7349 (1993).
23. Tanré, D., Kaufman, Y. J., Herman, M. & Matoo, S. Remote sensing of aerosol over oceans using the EOS-MODIS spectral radiances. *J. Geophys. Res.* **102**, 16971–16988 (1997).
24. Kaufman, Y. J. *et al.* Remote sensing of tropospheric aerosol over land from EOS moderate resolution imaging spectroradiometer. *J. Geophys. Res.* **102**, 17051–17068 (1997).
25. Reale, A. L., Chalfant, M. W., Wagoner, R. V., Gardner, T. J. & Casey, L. W. TOVS Operational Sounding Upgrades 1990–1992. *NOAA Tech. Rep. NESDIS 76* (US Dept of Commerce, NOAA NESDIS, Washington DC, 1994).

Acknowledgements. This study was supported by the US–Israel Binational Science Foundation. During some of this work, P.A. held a National Research Council–NASA/GSFC research associateship. Our thanks to Y. Banjamini for statistical help with Fig. 4.

Correspondence should be addressed to P.A. (e-mail: pinhas@cyclone.tau.ac.il).

Evidence for long-term diffuse deformation of the lithosphere of the equatorial Indian Ocean

Richard G. Gordon*, Charles DeMets† & Jean-Yves Royer‡

* *Department of Geology & Geophysics, Rice University, Houston, Texas 77005, USA*

† *Department of Geology & Geophysics, University of Wisconsin, Madison, Wisconsin 53706, USA*

‡ *Géosciences Azur, CNRS UMR 6526, BP48, 06235 Villefranche-sur-Mer cedex, France*

The presence of large earthquakes, east–west-striking folds and thrust faults in sediments, and east–west-striking undulations of wavelength 200 km in topography and gravity shows that the equatorial Indian Ocean is the locus of unusual deformation[1–8]. This deformation has been interpreted as a diffuse boundary between two tectonic plates[9–13]. Seismic stratigraphy and deep-sea drilling at two locations in the Bengal fan indicate that the deformation began 7.5–8.0 Myr ago[3,14,15]. Here, however, we show, using plate reconstructions, that motion across this diffuse oceanic plate boundary began more than 10 Myr earlier than previously inferred and that the amount of north–south convergence across the boundary through the central Indian basin has been significantly greater than the convergence estimated from seismic profiles. The relative plate velocity accommodated across the central Indian basin has varied with time and has been as fast as ~6 mm yr^{-1}—about half the separation rate of Earth's slowest-spreading mid-ocean ridge. The earliest interval of measurable motion, which began more than 18 Myr ago, may coincide with rapid denudation of the Tibetan plateau from ~21 Myr to 15–17 Myr (ref. 16). The present motion across the central Indian basin began no earlier than 11 Myr—following an earlier interval of slower motion from 18 to 11 Myr—and may have begun at ~8 Myr, when the Tibetan plateau is thought to have attained its maximum elevation[16,17].

The traditionally defined Indo-Australian plate is a composite plate comprising three distinct plates and many deforming zones that can be usefully treated as diffuse plate boundaries[13] (Fig. 1). Most studies of distributed lithospheric deformation in the Indian Ocean have focused on the equatorial region south of India. Deformation in this zone accommodates motion mainly between the Indian and Capricorn plates but also between these two plates and the Australian plate[13] (Fig. 1). Two major unconformities, revealed by an extensive network of seismic profiles, can be traced across the Bengal fan[3]. The age of the younger unconformity coincides with the onset of the folding and faulting that continues today[3]. This unconformity, which has been drilled in two places separated by ~1,100 km (Fig. 2), is 7.5–8.0 Myr old[3,14,15] and may coincide with the onset of normal faulting in the Tibetan plateau at ~8 Myr (ref. 16), when the plateau is believed to have first attained an elevation that equals or exceeds its present elevation[16,17]. The attainment of maximum elevation may in turn be related to significant climate change at 6–8 Myr, including the intensification of the monsoon over the Arabian Sea[18,19] and warming, increased aridity, and a change from forests to grasslands in northern Pakistan[20]. Molnar *et al.*[17] argue that the maximum elevation of the Tibetan plateau was attained only after its lithospheric mantle was convectively destabilized and removed. They further hypothesize that the resulting uplift and increase of potential energy of the plateau provided the large force required to cause folding of the Indo-Australian lithosphere, which occurs only if the force per unit length exceeds $\sim 4 \times 10^{12}$ N m^{-1} (ref. 17).

Here we present estimates of the motion of the Indian plate relative to the Capricorn plate since 18 Myr and since 20 Myr, and compare them with each other and with published estimates of the motion since 3 Myr (ref. 12) and 11 Myr (ref. 21). The reconstructions are determined from 81 crossings of the young end of anomaly 5E (18.3 Myr; ref. 22), 102 crossings of the old end of anomaly 6 (anomaly 6no, 20.1 Myr; ref. 22), 125 crossings of fracture zones near anomaly 5E, and 101 crossings of fracture zones near anomaly 6no flanking the central Indian and Carlsberg ridges. We used the 2-minute gravity grid of Sandwell and Smith[23] to select fracture zone crossings at 15-km intervals along the gravity troughs that we assume mark the axis of the fracture zones. Finite rotations between plates and the uncertainties in the rotations are determined using methods described by Royer and Chang[11].

Our plate reconstructions show that there is a large and obvious difference between the rotation of the Indian plate relative to the Capricorn plate since 20 Myr and the rotation since 11 Myr (Fig. 3). We rigorously tested whether India-Capricorn motion since chron 6 (20 Myr) exceeds that since chron 5 (11 Myr) by differencing the

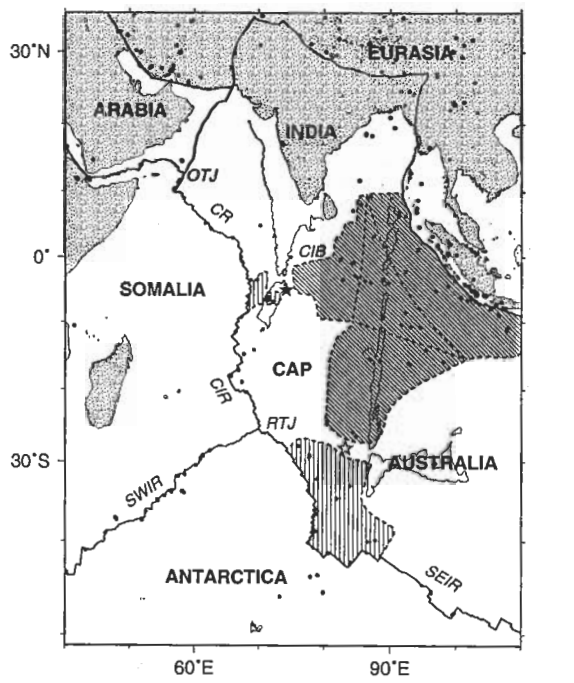

Figure 1 Location map. Small filled circles show the locations of earthquakes with magnitudes ≥5. The filled star shows the approximate pole of present rotation between the Indian and Capricorn plates; the open star shows the approximate pole of present rotation between the Capricorn and Australian plates. Vertically striped regions are diffuse plate boundaries across which divergence is accommodated; the diagonally striped region shows diffuse plate boundaries across which convergence is accommodated. Abbreviations: CAP, Capricorn plate; OTJ, Owen triple junction, CR, Carlsberg ridge; CIB, central Indian basin; CIR, central Indian ridge; RTJ, Rodrigues triple junction; SEIR, southeast Indian ridge; SWIR, southwest Indian ridge.

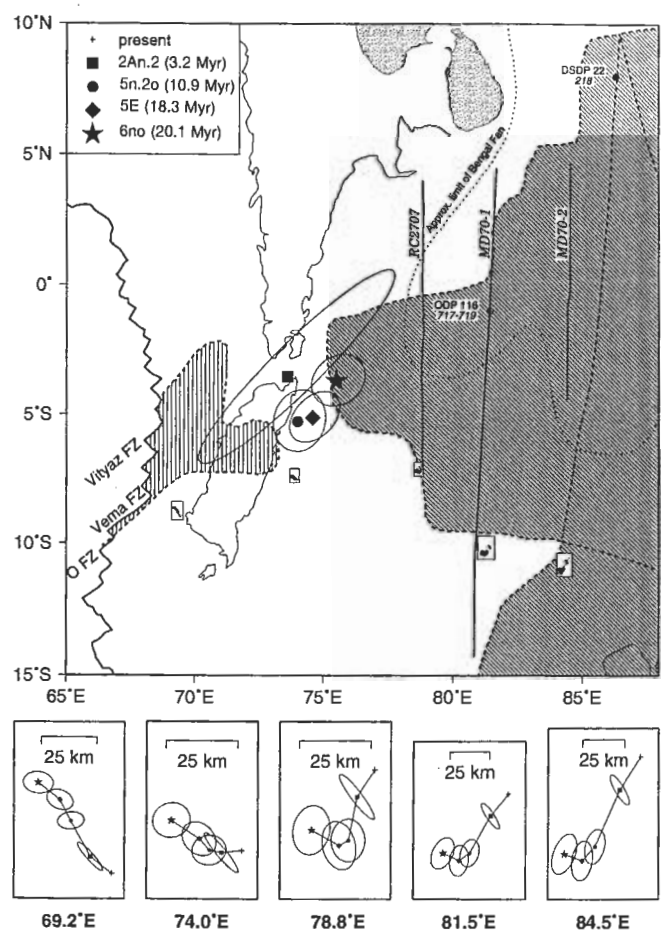

Figure 2 Map of equatorial Indian Ocean showing poles of finite rotation (and 95% confidence regions) between the Indian and Capricorn plates. The three north–south-striking lines labelled RC2707, MD70-1 and MD70-2 show the locations of seismic profiles along which north–south convergence has been estimated[5–7]. The location of ocean drilling sites (Site 218 from DSDP Leg 22 and Sites 717–719 from ODP Leg 116) are shown by circles with plus signs. Each of the five small rectangles in the top panel shows the reconstructed position of a point on the Capricorn plate relative to an arbitrarily fixed Indian plate; enlarged versions of these rectangles with their reconstructed points and 95% confidence regions are shown below the top panel. The reconstructions for anomaly 2A (3.2 Myr; ref. 22) and the old end of anomaly 5 (anomaly 5n.2o; 10.9 Myr; ref. 22) are modified from DeMets *et al.*[12] and Royer *et al.*[21], respectively. For each reconstruction, the chron identification, pole latitude (° N), pole longitude (° E), rotation angle (degrees), and the *xx*, *xy*, *xz*, *yy*, *yz*, and *zz* components of the covariance matrix are given in Table 1.

Table 1 Finite rotations and covariances

Chron	Pole location		Ω	Covariance matrix					
	Lat. (°N)	Long. (°E)	(deg.)	*xx*	*xy*	*xz*	*yy*	*yz*	*zz*
India-Somalia									
2An.2	26.23	28.14	−1.226	126.6	221.2	−96.3	488.5	−101.7	124.2
5n.2o	24.40	30.36	−4.349	354.7	744.5	19.2	1675.2	59.3	27.0
5E	24.22	32.25	−7.880	355.0	821.2	0.7	2074.6	29.6	20.9
6no	25.30	30.65	−8.488	551.2	1243.1	30.6	3012.3	83.0	35.8
Capricorn-Somalia									
2An.2	14.57	48.74	−1.927	75.4	148.7	−61.4	545.7	−83.0	63.1
5n.2o	13.67	47.07	−6.319	327.6	794.7	−235.9	2149.9	−615.4	199.6
5E	15.92	44.44	−10.239	557.6	1317.4	−340.6	3487.2	−820.5	241.8
6no	17.44	43.26	−10.861	395.6	968.9	−259.4	2774.2	−642.1	192.1
India-Capricorn									
2An.2	−3.54	73.60	0.922	389.7	436.5	−272.3	819.3	−263.3	214.4
5n.2o	−5.27	73.99	2.625	696.3	1555.4	−218.3	3816.4	−546.4	221.2
5E	−5.12	74.59	3.230	936.0	2162.6	−337.6	5550.9	−769.1	250.1
6no	−3.69	75.50	3.345	968.6	2235.1	−228.3	5775.4	−542.4	217.2

Ω is rotation angle; positive rotation angles are right-handed. Each rotation reconstructs the first-named plate relative to the second. The last six columns give the indicated elements of the covariance matrix in units of 10^{-8} rad^2 with the *x*, *y* and *z* axes being parallel to (0° N, 0° E), (0° N, 90° E) and 90° N, respectively.

India-Capricorn rotations for these two ages while propagating the errors[11]. A χ^2 test comparing this rotation with the null rotation gives a value of χ^2 of 78.3 with 3 degrees of freedom. The probability of obtaining a value this large or larger by chance if there were no motion between the Indian and Capricorn plates before 11 Myr is 1 in 7×10^{16}. An even greater minimum age of onset of motion between the Indian and Capricorn plates is obtained by differencing India-Capricorn rotations since the young end of chron 5E (18 Myr) and since the old end of chron 6 (20 Myr). A χ^2 test comparing this difference in rotations with the null rotation gives a value of χ^2 of 13.2 with 3 degrees of freedom. The probability of obtaining a value this large or larger by chance if there were no motion between the Indian and Capricorn plates before 18 Myr is 1 in 4×10^3. Thus motion began before 18 Myr, at least 10 Myr before the age of onset of deformation (7.5–8.0 Myr) inferred previously.

Our minimum age for the onset of India-Capricorn motion implies that deformation began somewhere in the equatorial Indian Ocean other than where the Bengal fan was drilled, or that the style of deformation changed at 7.5–8.0 Myr, or both. Our results are consistent with an onset of deformation of Indo-Australian lithosphere at ~20 Myr, coincident with the onset of rapid denudation of the Tibetan plateau from ~21 to ~15–17 Myr as indicated by thermochronometry[24,25], Sr isotopic evolution of sea water[26], and the sedimentary record of the Siwalik Group and the Bengal fan[27–29]. Our reconstructions indicate that motion across the central Indian basin was faster (~6 mm yr^{-1} to the ESE for a point now at 10° S, 81.5° E on the Capricorn plate) from 20 to 18 Myr, possibly coinciding with the episode of rapid denudation of the Tibetan plateau, than from 18 to 11 Myr when motion was slow (~1 mm yr^{-1} to the NE; Fig. 2). Our results are, however, also consistent with Indo-Australian deformation having started even earlier.

The Indo-Australian plate is believed to have come into existence shortly after chron 20 (43 Myr) when spreading between the Indian and Australian plates ceased in the Wharton basin[30]. Therefore, the Indo-Australian plate existed as a single nearly rigid plate for at most ~20 Myr and may never have existed at all. These alternatives may be testable by accurately reconstructing the motion between the Indian and Capricorn plates at one or more ages long before 20 Myr. In any event, our results show that the deformation of equatorial Indian Ocean lithosphere is not ephemeral, but long-lived.

The north–south component of convergence across the central Indian basin has been estimated from the throws and dips of thrust faults observed on north–south seismic profiles[5–7] (Figs 2, 4). The plate reconstructions indicate that the convergence since both chron 5E and chron 6 exceeds that estimated from each seismic profile (Fig. 4). If the seismic profiles record all the north–south shortening along them, as has been assumed in previous work, then our results would be inconsistent with the convergence estimates from the profiles. If instead we assume that the estimates from seismic profiles are only measuring the convergence since 7.5–8.0 Myr, then these estimates may be consistent with those from the plate reconstructions. Ideally the estimates from seismic profiles would be compared with those for plate motion since 7.5–8.0 Myr. Unfortunately there is no reconstruction available for this age. Instead we compare the convergence estimated from each seismic profile to those since 11 Myr. The ratio of the convergence estimated from seismic profiles to the convergence estimated from chron 5 plate reconstructions is 0.45, 0.77 and 0.82 along 78.8° E, 81.5° E and 84.5° E, respectively. The last two ratios are similar to the ratio, 0.69–0.73, of the assumed age of onset of the deformation estimated from the seismic profiles (7.5–8.0 Myr) to the old end of chron 5 (10.9 Myr). This leaves the discrepancy between the convergence estimates along 78.8° E to be explained, perhaps because the faults are listric and perhaps because of motion out of the vertical plane of the seismic profile.

Is some tectonic event other than the onset of motion between the Capricorn and Indian plates recorded by the seismic stratigraphy and ocean drilling? Perhaps it is an acceleration of motion across the central Indian basin and the onset of a particular mode of deformation, the lithosphere-scale folding and associated thrust faulting and small-scale folding that presumably continue today. The rate of motion accommodated across the central Indian basin was slow (~1 mm yr^{-1}) from 18 to 11 Myr, but increased to ~4 mm yr^{-1} to the NNE (near 10° S, 81.5° E) between 11 Myr and 3 Myr, and further increased to ~6 mm yr^{-1} to the NNE since 3 Myr. Thus, the constraints from the plate reconstructions are consistent with plate motion across the central Indian basin having accelerated at ~8 Myr, when the Tibetan plateau is believed to have attained its maximum elevation. Additional plate reconstructions for ages between 11 Myr and 3 Myr could bracket the timing more closely. In any event, the force that deformed the diffuse plate boundary before ~8 Myr must have been too small, in the wrong direction, or both, to cause lithosphere-scale folding. Our reconstructions indicate that, on average, points on the Capricorn plate in the southern central Indian basin moved mainly to the east from ~20 to ~11 Myr, and moved to the NNE since that time (see the points at 78.8° E, 81.5° E and 84.5° E in Fig. 2). If the boundary before 11 Myr was also an east–west-striking zone, as is the present boundary, the deformation that occurred before 11 Myr ago was east–west simple shearing. □

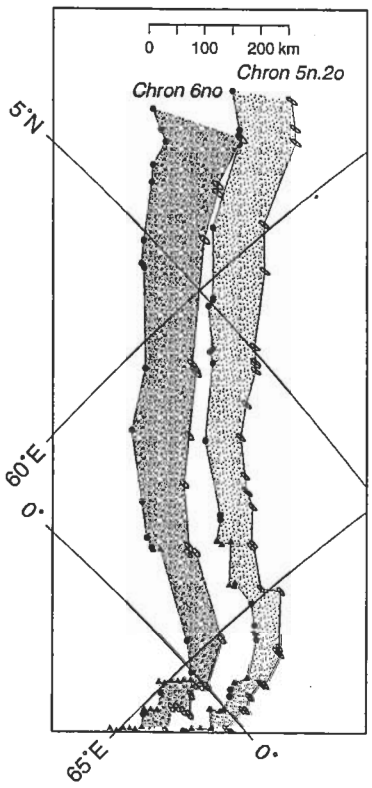

Figure 3 Reconstructions of magnetic anomalies 6 and 5 along the Carlsberg ridge. Locations of crossings of the old end of magnetic anomalies 6 (anomaly 6no; left) and 5 (anomaly 5n.2o; right) on the Somalian plate, which is arbitrarily held fixed, are shown as filled circles; associated fracture crossings are shown as filled triangles. A thin line connects the Somalian 6no crossings and another thin line connects the Somalian 5n.2o crossings. Coeval Indian plate magnetic anomaly and fracture zone crossings, which are shown by their 95% confidence ellipses, have been reconstructed using the appropriate rotation that best fits the Capricorn plate to the Somalian plate for either chron 6no or chron 5n.2o. Each set of Indian crossings is also connected by a thin solid line. The stippled region on the left shows the gap between the Somalian plate and Indian plate crossings for chron 6no, whereas the stippled region on the right shows the gap for chron 5n.2o. If India and Capricorn were part of a single rigid plate, the Somalian and Indian crossings would coincide in location within their uncertainties. The gaps shown here are caused by the neglect of the motion between the Indian and Capricorn plates. If the motion between the Indian and Capricorn plates occurred entirely since chron 5n.2o (10.9 Myr; ref. 22), as would be the case if motion began 7.5–8.0 Myr as inferred from seismic stratigraphy and drilling in the Bengal fan[15], the chron 6no (20.1 Myr; ref. 22) gap would be the same within uncertainties as the chron 5n.2o gap. The chron 6no gap is significantly larger, however, than the chron 5n.2o gap. The former is as large as ~140 km along the northwestern Carlsberg ridge (top of panel), wheres the latter is only as large as ~100 km. The figure is an oblique Mercator projection about the India-Somalia stage pole rotation from chron 6no to chron 5n.2o.

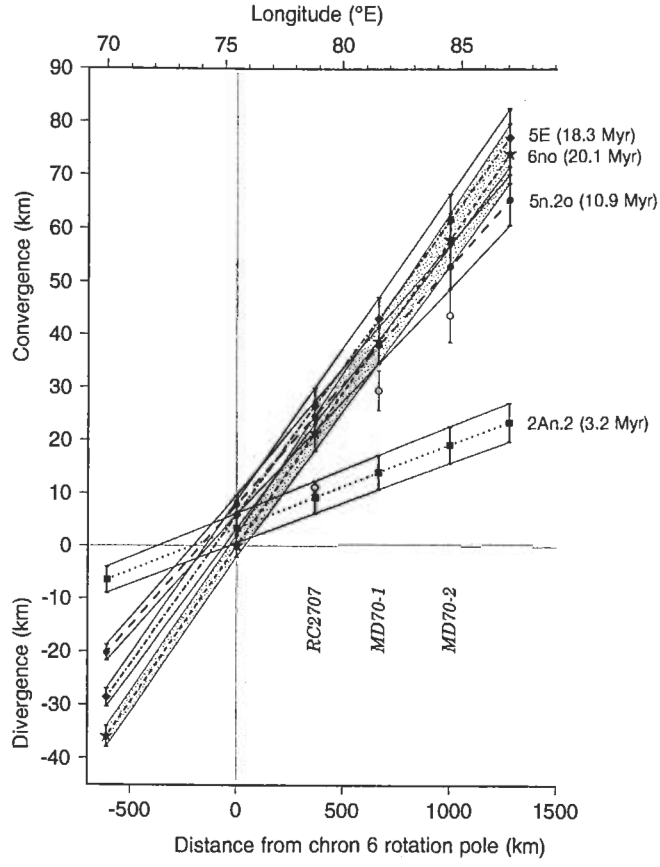

Figure 4 Estimated north–south convergence or divergence between the Indian and Capricorn plates. Convergence or divergence inferred from plate reconstructions (filled symbols) are shown for lines that are now north–south in the equatorial Indian Ocean since the middle of chron 2A[12] (3.2 Myr), the old end of chron 5[21] (chron 5n.2o; 10.9 Myr), the young end of chron 5E (18.3 Myr), and the old end of chron 6 (chron 6no; 20.1 Myr). Also shown are estimates of convergence from north–south seismic lines along 78.8° E, 81.5° E, and 84.5° E (open circles)[5–7]. Vertical bars show $\pm 1\sigma$ errors. The convergence since 3.2 Myr is less than estimated along each seismic profile, but insignificantly so along 78.8° E, whereas the convergence since 10.9 Myr is greater than that along each profile, significantly so only along 78.8° E[21]. The convergence since chron 5E and since chron 6 exceeds that estimated along every seismic profile: 27.1 ± 6.7 km (5E) and 22.5 ± 6.5 km (6) versus 11 ± 2 km (ref. 7) along 78.8° E, 43.8 ± 8.0 km (5E) and 39.9 ± 8.0 km (6) versus 29.5 ± 7.5 km[5] along 81.5° E, and 62.3 ± 9.4 km (5E) and 59.1 ± 9.6 km (6) versus 44 ± 10 km (ref. 6) along 84.5° E. Averaging the north–south convergence estimated from the 5E and 6 plate reconstructions and then subtracting the north–south convergence estimated from seismic profiles gives the following differences: 13.6 ± 5.0 km along 78.8° E, 12.3 ± 9.4 km along 81.5° E, and 16.7 ± 12.0 km along 84.5° E. (Here all values after '±' symbols are 95% confidence limits.)

Received 19 November 1997; accepted 11 June 1998.

1. Stein, S. & Okal, E. A. Seismicity and tectonics of the Ninetyeast Ridge area: Evidence for internal deformation of the Indian plate. *J. Geophys. Res.* **83**, 2233–2245 (1978).
2. Weissel, J. K., Anderson, R. N. & Geller, C. A. Deformation of the Indo-Australian plate. *Nature* **287**, 284–291 (1980).
3. Curray, J. R. & Munasinghe, T. Timing of intraplate deformation, northeastern Indian Ocean. *Earth Planet. Sci. Lett.* **94**, 71–77 (1989).
4. Bull, J. M. & Scrutton, R. A. Seismic reflection images of intraplate deformation, Central Indian Ocean, and their tectonic significance. *J. Geol. Soc. Lond.* **149**, 955–966 (1992).
5. Chamot-Rooke, N., Jestin, F., de Voogd, B. & Phèdre Working Group Intraplate shortening in the central Indian Ocean determined from a 2100-km-long north-south deep seismic reflection profile. *Geology* **21**, 1043–1046 (1993).
6. Jestin, F. *Cinématique rigide et Déformations dans la Jonction Triple Afar et dans le Basin Indien Central.* Thesis, Univ. Pierre et Marie Curie (Paris 6) (1994).
7. Van Orman, J., Cochran, J. R., Weissel, J. K. & Jestin, F. Distribution of shortening between the Indian and Australian plates in the central Indian Ocean. *Earth Planet. Sci. Lett.* **133**, 35–46 (1995).
8. McAdoo, D. C. & Sandwell, D. T. Folding of oceanic lithosphere. *J. Geophys. Res.* **90**, 8563–8569 (1985).
9. Wiens, D. A. *et al.* A diffuse plate boundary model for Indian Ocean tectonics. *Geophys. Res. Lett.* **12**, 429–432 (1985).
10. Gordon, R. G., DeMets, C. & Argus, D. F. Kinematic constraints on distributed lithospheric deformation in the equatorial Indian Ocean from present motion between the Australian and Indian plates. *Tectonics* **9**, 409–422 (1990).
11. Royer, J.-Y. & Chang, T. Evidence for relative motions between the Indian and Australian plates during the last 20 Myr from plate tectonic reconstructions: Implications for the deformation of the Indo-Australian plate. *J. Geophys. Res.* **96**, 11779–11802 (1991).
12. DeMets, C., Gordon, R. G. & Vogt, P. Location of the Africa-Australia-India triple junction and motion between the Australian and Indian plates: Results from an aeromagnetic investigation of the central Indian and Carlsberg ridges. *Geophys. J. Int.* **119**, 893–930 (1994).
13. Royer, J.-Y. & Gordon, R. G. The motion and boundary between the Capricorn and Australian plates. *Science* **277**, 1268–1274 (1997).
14. Moore, D. G., Curray, J. R., Raitt, R. W. & Emmel, F. J. Stratigraphic-seismic section correlations and implications to Bengal Fan history. *Initial Rep. DSDP* **22**, 403–412 (1974).
15. Cochran, J., Stow, D. & Leg 116 shipboard scientific party Collisions in the Indian Ocean. *Nature* **330**, 519–521 (1987).
16. Harrison, T. M., Copeland, P., Kidd, W. S. F. & Yin, A. Raising Tibet. *Science* **255**, 1663–1670 (1992).